Fat-Free MRI Based on Magnetization Exchange

Jin-Hong Chen,[1] H. Carl Le,[2] Jason A. Koutcher,[2] and Samuel Singer[1*]

An MRI technique is proposed for complete fat signal elimination. This approach exploits the fact that water rapidly exchanges magnetization with protons in protein and membrane phospholipid of tissue and cells but does not exchange magnetization with triglyceride or fat protons in the tissue. Saturation of the proton signal from protein and membrane phospholipid thus results in partial saturation of the water proton signal, allowing acquisition of an image including a portion of the water signal and the full fat signal. Subtraction of this image from the standard image, containing both water and fat signals, results in an image in which all fat signal is cancelled. This fat-free image is sensitive to magnetization transfer and to water density and relaxation time, providing the possibility of additional contrast. Unlike most fat suppression techniques, this method is not compromised by the static or radiofrequency field heterogeneity and is equally efficient for all fat resonances independent of their chemical shift frequency. Magn Reson Med 63:713–718, 2010. ©2010 Wiley-Liss, Inc.

Key words: Fat suppression; magnetization transfer; fat-free MRI; fat images; fat spectrum

Water and fat (triglyceride) are the two major signal sources in MRI. Fat signals can compromise MRI quality by overwhelming the water images in fat-abundant regions. A strong fat signal can also impede the precision of tumor detection by inducing chemical shift artifacts and by obscuring the effects of MRI relaxation agents, which interact only with water (1,2). Therefore, fat-suppression and water- or fat-selective imaging have been used in many routine clinical examinations to reduce artifacts and to improve tissue characterization (3). Experimental techniques to achieve these goals include direct presaturation on the large fat methylene peak (4,5), selective suppression of fat based on the T_1 relaxation time difference between water and fat signal (6–8), selective excitation of water using selective pulses (9–11), and the 'Dixon method', which works with phase shifts (12,13). These methods can be very sensitive to the heterogeneity of the amplitude of the static field and/or the radiofrequency (RF) field (3). Furthermore, the majority of these schemes consider fat to have only a single resonance or assume that all the fat signals have a uniform relaxation time. In reality, fat triglyceride comprises 10 resonances that are spread over a chemical shift range of more than 4.4 part per million (ppm) from the vinyl peak to the methyl peak. The strongest peak is the methylene on the triglyceride fatty acid chains, excluding those methylene groups that are one bond away from the vinyl group and those one or two bonds away from the carbonyl group. This large methylene peak accounts for approximately 60% of all the fat signals. The remaining 40% of fat signals have been ignored in most fat-suppression techniques; this can induce image artifacts and compromise image interpretation. The problem is typically more pronounced at higher magnetic field.

Here we show a new approach for fat suppression that completely eliminates all the fat signals irrespective of their chemical shift frequency and that is insensitive to the heterogeneity of RF field and static field. This new approach relies solely on the fact that fat protons do not exchange magnetization with water or with protein and cell membrane phospholipids protons in tissue samples (14). This method extends the classic MRI magnetization transfer (15–17) technique and generates a fat-free image that is sensitive to magnetization transfer, as well as the tissue water density and relaxation time.

MATERIALS AND METHODS

Approach for Elimination of the Fat Signal

Figure 1 illustrates our experimental approach. Figure 1a shows the basic magnetization transfer network in tissue for the three components relevant to our approach: tissue protein and membrane phospholipid, water, and fat. Magnetization transfer between fat and water, and between fat and the protons of tissue protein and membrane phospholipid, either does not exist or is extremely weak and not detectable with current NMR methods (14). In contrast, magnetization transfer between water and the tissue protein and membrane phospholipid proton component is complex but highly efficient. This magnetization transfer network suggests that presaturation of this tissue proton component will have no effect on the fat signal but will partially or fully saturate the water signal due to magnetization transfer from water to the tissue protein and membrane phospholipid protons. On static state NMR analysis, the resonance from tissue protein and membrane phospholipid protons has a line width that exceeds 2000 Hz (18,19). The proton signal from this tissue component is thus too broad to be seen in the static NMR spectrum and does not contribute to the MRI signal. Selective presaturation of the protein and membrane phospholipid tissue protons is easy to

[1]Sarcoma Disease Management Program, Memorial Sloan-Kettering Cancer Center, New York, New York, USA.

[2]Medical Physics, Memorial Sloan-Kettering Cancer Center, New York, New York, USA.

Grant sponsor: Soft Tissue Sarcoma Program Project; Grant number: PO1 CA047179. Grant sponsor: National Institutes of Health; Grant number: NIH P30 CA08748 and U24CA83084.

*Correspondence to: Samuel Singer, M.D., MSKCC Room H-1220, 1275 York Avenue, New York, NY 10065. E-mail: singers@mskcc.org

Received 26 February 2009; revised 20 July 2009; accepted 21 August 2009.

DOI 10.1002/mrm.22208

Published online 9 February 2010 in Wiley InterScience (www.interscience.wiley.com).

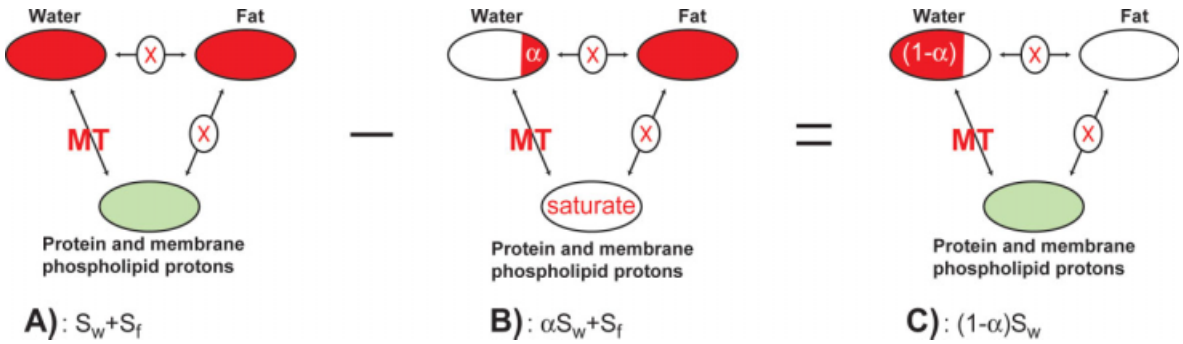

FIG. 1. Scheme of fat-free imaging based on the magnetization exchange network for the three relevant components. **a:** Signal (red) of a regular image including water and fat. Also shown is the magnetization exchange network. Magnetization transfer between water and tissue protein and membrane phospholipid protons is efficient. Fat does not exchange magnetization with water or with the tissue proton component. **b:** Signal of the image with presaturation of tissue protein and membrane phospholipid protons. Presaturation of tissue proton component also saturates water signal but has no influence on the fat signal. **c:** A fat-free, water-only image is obtained by the subtraction of the image represented by **(b)** from the image represented by **(a)**.

implement; for example, by using a low-power, long-time irradiation at any position along the broad spectral resonance frequency of this tissue proton component (15,16), as long as it is not on water or fat signals.

The method outlined in Fig. 1 is further described using a simple mathematical model. The signal of a regular image (schematized in Fig. 1a) includes both water and fat signals:

$$s_A = s_w + s_f \quad [1]$$

Here, s_w and s_f are the image signals from water and fat, respectively. This image can be acquired using any approach that is best suited to the particular application. Therefore, signals s_w and s_f can be sensitive to water density and fat and water relaxation times.

Figure 1b schematizes a second image acquired with the tissue protein and membrane phospholipid protons presaturated. This presaturation does not change any of the fat signals because there is no magnetization transfer from fat to water or to the tissue proton component. Magnetization transfer from water to the tissue protein and membrane phospholipid protons will reduce the water signal to αs_w, where α describes the proportion of the water signal that remains. Consequently, the signal acquired in Fig. 1b consists of the full fat signal and a portion of the water signal:

$$s_B = \alpha s_w + s_f \quad [2]$$

Factor α depends on the efficiency of magnetization transfer between water and the tissue protein and membrane phospholipid protons and is determined mainly by the magnetization transfer rate between water and these tissue protons, the relaxation rates of water and these tissue protons, and the irradiation time and intensity of the pulse used to presaturate the tissue proton component (20–23). Factor α can be experimentally determined for a specific tissue.

A subtraction of the two images represented by Eq. 1 and Eq. 2 results in the final image schematized in Fig. 1c:

$$s_C = (1-\alpha)s_W \quad [3]$$

All the fat signals are eliminated irrespective of their chemical shift.

This method is independent of the heterogeneity of the static or RF field. In the water-only image that is proportional to $(1-\alpha)s_w$, the magnetization transfer factor $(1-\alpha)$ provides magnetization transfer contrast (15,16) in addition to the contrast provided by water density or relaxation time embedded in the image signal s_w.

If the factor α is estimated by an independent experiment, an image that consists only of fat signal can be determined from Eq. 1 and Eq. 2 as

$$\alpha s_A - s_B = (\alpha - 1)s_f \quad [4]$$

This fat-only image contains signals from all fat resonances. If α approaches 0, this calculation is unnecessary; Fig. 1b is a fat-only image.

Tissue Sample Experiments

Experiments were carried out on a Bruker Avance 600 MHz spectrometer (Bruker Biospin, Billerica, MA) and on a 5mm probe with x, y, and z triple gradients. The samples were surgically resected human fat tissue and well-differentiated liposarcoma tissue. Specimens were obtained with consent of the patients and with institutional review board approval. Each tissue sample was cut into small pieces. The small pieces were then drawn into a capillary tube (inner diameter 1mm; outer diameter 1.8 mm) by attaching the capillary to a syringe. In aggregate, these small tissue pieces occupied about a 1-cm-long length of the capillary tube. One end of the capillary was then sealed with a small piece of polytetrafluoroethylene seal tape. A second capillary filled with heavy water (D_2O) for field-frequency lock was placed parallel with the sample capillary into the 5mm tube. The samples were maintained at 20°C during experiments.

The fat-suppression method was applied to both spectra and images. The images were acquired using presaturation and gradient echo with presaturation power off

and on, respectively. Detailed parameters for imaging are listed in the figure caption. To clearly illustrate the imaging results, a small field of view was used. For spectroscopy, a 90° pulse with presaturation was used. The spectra were acquired using eight scans, 16,000 data points. The spectrum was acquired on the whole tissue, and the thickness of the image slice was 5.5 mm.

For both imaging and spectroscopy, the RF frequency was at 8.3 ppm for presaturation and was moved to 4.7 ppm for pulsing and data acquisition. The presaturation pulse was 5 sec long, with an intensity of approximately 100 Hz.

Obese Mouse Imaging

The experiments were carried out on an obese mouse (model number OB-M-F, Taconic Farms Inc, Hudson, NY) under a protocol approved by Memorial Sloan-Kettering Cancer Center Research Animal Resource Center. Images were acquired on a 7.05-T Bruker Biospec Spectrometer using a birdcage coil. A coronal image was acquired with rapid acquisition with relaxation enhancement (RARE) (24) and presaturation. Imaging parameters included echo time = 35 ms, pulse repetition time = 2665 ms, field of view 4.2 × 5.6 cm, matrix 256 × 256, slice thickness of 1.06 mm, and total imaging time of 20 min.

The pulse used to selectively presaturate the tissue protein and membrane phospholipid protons consisted of 250 repetitions of (10 ms gaussian pulse–10 ms blank) with total length of 5 sec and an average intensity of approximately 110 Hz for the gaussian pulse. Two images were acquired, with the presaturation power off and on, to allow for a subtraction to obtain the fat-free image. As in the above tissue experiment, the RF frequency was at 8.3 ppm for presaturation and was moved to 4.7 ppm for pulsing and data acquisition.

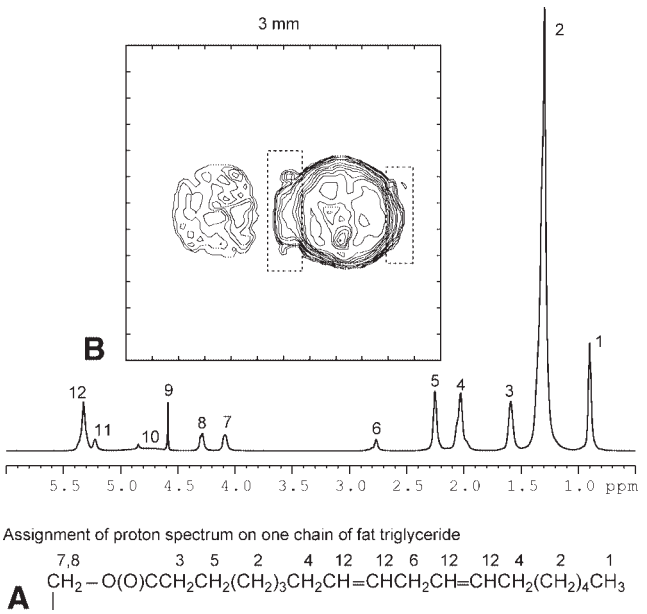

FIG. 2. Spectrum and contour-plot image acquired on a fat tissue sample in a capillary tube. **a:** Spectrum, with the peaks numbered and assigned on one chain of the triglyceride molecule (the remainder of the triglyceride is not shown). Peak 10 is from water in the tissue. Peak 9 is the residual water in D_2O in the capillary tube that was placed parallel to the tissue sample tube. Peak 11 is from the glycerol proton of the middle triglyceride chain (not shown in triglyceride molecule diagram). **b:** Image acquired using gradient echo. The figure shows a slice from the center of a cylindrical sample 1mm in diameter. The two images are separated by 1.1mm. The parameters to acquire the image: G_s, 2.4 gauss/cm × 1 ms; G_f, 4.7 gauss/cm, $G\phi$, 7.5 gauss/cm × 2 ms with 256 steps; 512 points per free induction decay. The image has 512 × 512 data points.

RESULTS

Dispersion of Fat Resonances and the Resulting Chemical Shift Artifact

It is well known that fat signals induce chemical shift artifacts into a water image (1–3). To illustrate these artifacts, we performed spectroscopy and imaging without fat elimination on a sample of human fat tissue. Fig. 2 shows the spectrum (Fig. 2a) and the contour-plot image (Fig. 2b) acquired on a sample loaded in a capillary tube with a diameter of 1mm on a 600-MHz (14 T) spectrometer. The water signal from the fat tissue (peak 10 and a small fairly broad peak under peak 10) was very small compared to the strong fat signals. The major methylene peak (peak 2) accounted for 59% of all fat signals in this sample. The vinyl signal (peak 12) was approximately 11% the intensity of peak 2.

The broad separation of fat resonances results in a chemical shift artifact, in which the signals originating from low resonances are misregistered in the image with respect to signals from high resonances (1–3). At high field, the resonance frequencies of the different fat signals show increased separation, which can further intensify this chemical shift problem. Thus, in Fig. 2b, which is an image generated at high field strength (14 T) and with a small field of view, it is not surprising that the various fat signals were misregistered, resulting in two images. The left image came from resonances 7, 8, 11, and 12 of fat. The small tissue water signal (resonance 10) also contributed slightly to this left image. The right image came from resonances 1, 2, 3, 4, 5, and 6, with the majority of signal generated from the methylene peak 2. The intensity of the left image is approximately 8.5% that of the right image. The 1.1mm separation of the two images is consistent with the 2419-Hz distance between vinyl peak 12 and methylene peak 2 in the spectrum at 600-MHz field and with the imaging parameters (applied reading gradient of 1.1 gauss/cm; acquisition sampling rate 40,000 Hz). In addition, the spread of the fat resonances 1, 3, 4, 5, and 6 around 2 generated extended edges on both sides of the right image (see the areas in the dashed rectangles), as evidenced by its shape being elliptical rather than circular. If conventional fat suppression were applied to remove the signal from peak 2, both images would persist, as would the extended edges around the right image.

Complete Elimination of Fat Signal in MRI of a Liposarcoma Sample

The magnetization transfer methodology for complete fat elimination was applied to sample of well-differentiated liposarcoma, a tumor type that typically contains

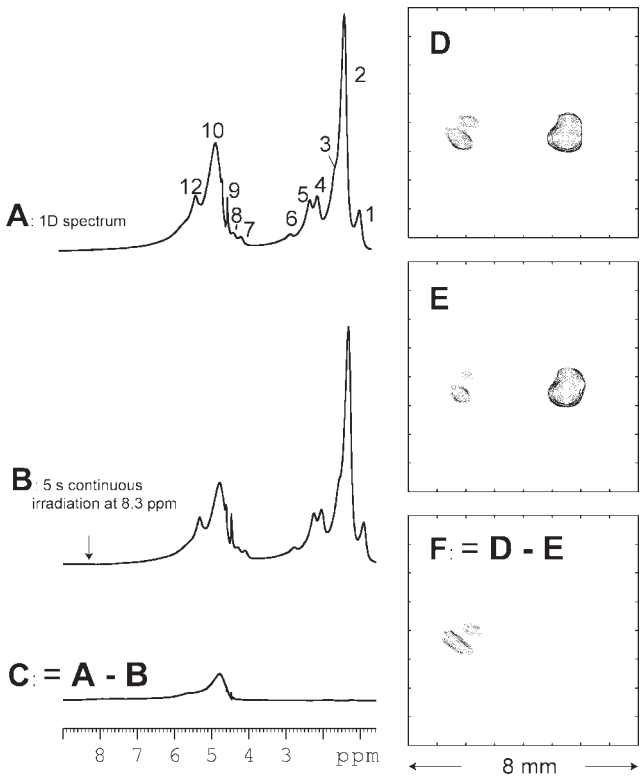

FIG. 3. Spectra and contour-plot images acquired on well-differentiated liposarcoma tissue in a capillary tube. Spectra **(a)** and **(b)** were acquired using 90° pulse and presaturation with the presaturation power off and on, respectively. The peaks are numbered as in Fig. 2. Spectrum **(c)** is the subtraction of spectrum **(b)** from **(a)**. **d-f:** Images of a single slice of the liposarcoma sample, which is 1mm in diameter. **(d)** And **(e)** were acquired using gradient echo and presaturation with the presaturation power off and on, respectively. **f:** The subtraction of **(e)** from **(d)**. The parameters to acquire the images: G_s, 6.0 gauss/cm × 1 ms; G_f, 1.3 gauss/cm, $G\phi$, 1.1 gauss/cm × 2 ms with 256 steps; 512 points per free induction decay. Each image has 512 × 512 data points.

triglyceride at a concentration around 5 M (see Fig. 3a). In this specimen, the water signal was weaker than the strong fat signal but was large enough to be imaged. The spectra (Fig. 3a-c) illustrate the concept of complete fat-suppression. The spectrum in Fig. 3a was acquired without presaturation and that in Fig. 3b was acquired with 5 sec presaturation at 8.3 ppm. The spectrum in Fig. 3c, which is the subtraction of the spectrum in Fig. 3b from 3a, shows clean elimination of all the fat signals.

As with the fat sample in Fig. 2, the liposarcoma sample was misregistered into two images, both in imaging with presaturation (Fig. 3e) and without presaturation (Fig. 3d). However, unlike the fat sample, for which both images were from fat because the sample contained very little water (Fig. 2b), in this well-differentiated liposarcoma the water signal (peak 10) was stronger than the vinyl peak from fat. Thus, the left images in Fig. 3d and e were mainly from water, though the vinyl and the glycerol proton resonances from fat also contributed. The right images in Fig. 3d and e were purely from the fat resonance, mainly from the methylene at 1.29 ppm. The images show that water signal was not spatially homogeneously distributed inside the tube. It is unknown if this nonhomogeneous distribution reflects the true nature of the tissue water or if it resulted from the sample preparation process with two distinct small pieces of liposarcoma tissue residing in an imaging slice from the same axial location in the capillary tube. The image in Fig. 3f is the subtraction of Fig. 3e from Fig. 3d. In Fig. 3f the large image from fat was completely eliminated.

MRI of an Obese Mouse

Application of this method on an imaging scanner is straightforward. Fig. 4 shows images from an obese mouse. Fig. 4a is a regular image acquired using RARE (24) with no presaturation pulse. This image displays large quantities of fat all over the body of the obese mouse. The signal intensities of kidney and liver are much weaker than that of fat. Fig. 4b was acquired using the same method, but with a presaturation pulse. The kidney signal was barely detectable, implying that the 5-sec irradiation of the tissue protein and membrane phospholipid proton component resulted in very efficient magnetization transfer from water. Figure 4c is the subtraction of Fig. 4b from Fig. 4a. We increased image brightness/contrast of Fig. 4c compared to Fig. 4a and b. In this fat-free image, fat suppression was uniform and the image contained no imaging artifacts. For kidney, the signal intensity of the subtracted image (Fig. 4c) was 85% of the standard image (Fig. 4a). The 15% reduction in signal intensity results from the magnetization transfer factor α and removal of the small fat signal that originates from the low fat levels present in kidney. The signal intensity for liver in Fig. 4c was reduced more than 50% from the standard image because the liver of this obese mouse contained a substantial amount of fat that was no longer detected in the fat-subtracted image (Fig. 4c).

DISCUSSION AND CONCLUSION

We have shown that fat signal can be completely eliminated from MR images by exploiting the absence of magnetization transfer from fat to water or to protein and membrane phospholipid protons. The method entails imaging with and without presaturation of the tissue proton component to suppress signal from water, and subsequent generation of a water-only image by subtraction. We demonstrated clean elimination of fat signals for a liposarcoma sample and an obese mouse. Both tissue sample and the obese mouse contained concentrations of triglyceride that exceeded 5 M and therefore represent an extreme for the amount of fat relative to water. This demonstrates that the proposed fat-suppression method can be applied to eliminate the fat signals for tissues with any fat content.

The fat-elimination method described is substantially more efficient at suppressing fat signal than the conventional fat-suppression and water- or fat-selective imaging methods. The major methylene signal is the focus of most traditional techniques for fat-suppression, water-selective imaging or fat-selective imaging, while the remaining resonances are ignored. For a regular triglyceride molecule including two double bonds in each of the three chains, the major methylene signal constitutes at

FIG. 4. Images acquired on an obese mouse. **a:** Image acquired using RARE and with the presaturation power off. **b:** Image acquired using RARE and with the saturation power on. **c:** Fat-free image consisting of the subtraction of **(b)** from **(a)** with adjustment of the image brightness/contrast level. The distorted external shape of the mouse resulted from using an undersized support structure to contain the oversized obese mouse in the imaging magnet.

most 65% of all the fat signals. Any increase in the double bond content of fat will further reduce the ratio of fat methylene signal to total fat signals in the sample. Therefore, traditional fat-suppression techniques that address only the major methylene signal fail to suppress at least 35% of the signal from fat. In addition, presaturation (4,5), which is among the most popular fat-suppression methods, will reduce the water signal intensity because saturation of the major methylene signal also partly saturates protein and membrane phospholipid signal, which triggers magnetization transfer from water.

Our fat-elimination approach offers several advantages. As shown in Fig. 4 of the obese mouse, we retained 85% of the kidney signal intensity. For most tissues other than fat, magnetization transfer from water to protein and membrane phospholipid protons is very efficient (α is very small), and thus in most tissues very little water signal is lost. Furthermore, the elimination of the fat signal does not depend on the chemical shift or the line width of the fat signals, and it is not affected by the heterogeneity of amplitude of static field or RF field. The magnetization exchange method can be utilized for any magnetic field strength, and an increase in magnetic field strength does not require any further modification to the approach. Finally, this approach can be combined with other MRI techniques.

The only drawback to this approach (which is shared by all fat-suppression methods that are based on the subtraction of two images) is the 2-fold increase in imaging time. However, the acquired water-only image provides additional information, as it is now sensitive to magnetization transfer in addition to the tissue water density or relaxation time. Magnetization transfer imaging is a well-developed methodology (16,17,25) and has been found useful in many applications such as magnetic resonance angiography (26), breast imaging (27), brain metabolism (28), and multiple sclerosis (29). The fat-free imaging method presented in this work retains all the advantages of traditional magnetization transfer contrast. It should further enhance contrast for more precise tissue characterization and tumor delineation, particularly for tumors arising in regions of high fat content such as the retroperitoneal space.

The magnetization transfer factor $(1 - \alpha)$ in Eq. 3 depends on many factors (20–23) but can be controlled by adjusting the intensity and length of the presaturation pulse. When the presaturation pulse is strong enough and long enough, $(1 - \alpha)$ are approximately the same for many tissue types (data are to be published in a future paper) and thus will not contribute contrast to the fat-free image. However, under standard imaging conditions, the intensity and length of the presaturation pulse are typically very limited, resulting in significantly different magnetization transfer rates for different tissue types and under these conditions will enable significant magnetization transfer contrast.

ACKNOWLEDGMENTS

The authors thank Rachael O'Connor for her assistance with the mouse experiments and Dov P. Winkleman for imaging the obese mouse on the 7-T scanner. This research was supported in part by the Kristen Ann Carr Fund and the Department of Surgery at MSKCC, and the soft tissue sarcoma Program Project P01 CA047179, and NIH P30 CA08748 and U24CA83084.

REFERENCES

1. Simon JH, Szumowski J. Proton (fat/water) chemical shift imaging in medical magnetic resonance imaging: current status. Invest Radiol 1992;27:865–874.
2. de Kerviler E, Leroy-Willig A, Clement O, Frija J. Fat suppression techniques in MRI: an update. Biomed Pharmacother 1998;52:69–75.
3. Delfaut EM, Beltran J, Johnson G, Rousseau J, Marchandise X, Cotten A. Fat suppression in MR imaging: techniques and pitfalls. Radiographics 1999;19:373–382.
4. Hoult DI. Solvent peak saturation with single phase and quadrature Fourier transformation. J Magn Reson 1976;21:337–347.
5. Keller PJ, Hunter WW Jr, Schmalbrock P. Multisection fat: water imaging with chemical shift selective presaturation. Radiology 1987; 164:539–541.
6. Bydder GM, Young IR. MR imaging: clinical use of the inversion recovery sequence. J Comput Assist Tomogr 1985;9:659–675.
7. Gyngell M. The steady-state signals in short-repetition-time sequences. J Magn Reson 1989;81:474–483.
8. Kaldoudi E, Williams SC, Barker GJ, Tofts PS. A chemical shift selective inversion recovery sequence for fat-suppressed MRI: theory and experimental validation. Magn Reson Imaging 1993;11:341–355.

9. Frahm J, Haase A, Hanicke W, Matthaei D, Bomsdorf H, Helzel T. Chemical shift selective MR imaging using a whole-body magnet. Radiology 1985;156:441–444.
10. Schick F, Bongers H, Jung WI, Skalej M, Lutz O. Localized Larmor frequency-guided fat and water proton MRI of the spine: a method to emphasize pathological findings. Magn Reson Imaging 1991;9: 509–515.
11. Schick F, Forster J, Machann J, Huppert P, Claussen CD. Highly selective water and fat imaging applying multislice sequences without sensitivity to B1 field inhomogeneities. Magn Reson Med 1997; 38:269–274.
12. Dixon WT. Simple proton spectroscopic imaging. Radiology 1984; 153:189–194.
13. Glover GH, Schneider E. Three-point Dixon technique for true water/ fat decomposition with B0 inhomogeneity correction. Magn Reson Med 1991;18:371–383.
14. Chen JH, Sambol EB, Decarolis P, O'Connor R, Geha RC, Wu YV, Singer S. High-resolution MAS NMR spectroscopy detection of the spin magnetization exchange by cross-relaxation and chemical exchange in intact cell lines and human tissue specimens. Magn Reson Med 2006;55:1246–1256.
15. Muller RN, Marsh MJ, Bernardo ML, Lauterbur PC. True 3-D imaging of limbs by NMR zeugmatography with off-resonance irradiation. Eur J Radiol 1983;3:286–290.
16. Balaban RS, Ceckler TL. Magnetization transfer contrast in magnetic resonance imaging. Magn Reson Q 1992;8:116–137.
17. Henkelman RM, Stanisz GJ, Graham SJ. Magnetization transfer in MRI: a review. NMR Biomed 2001;14:57–64.
18. Feigenson GW, Chan SI. Nuclear magnetic relaxation behavior of lecithin multilayers. J Am Chem Soc 1974;96:1312–1319.
19. Forbes J, Husted C, Oldfield E. High-field, high-resolution proton "magic-angle" sample: spinning nuclear magnetic resonance spectroscopic studies of gel and liquid crystalline lipid bilayers and the effects of cholesterol. J Am Chem Soc 1988;110:1059–1065.
20. Pike GB. Pulsed magnetization transfer contrast in gradient echo imaging: a two-pool analytic description of signal response. Magn Reson Med 1996;36:95–103.
21. Eng J, Ceckler TL, Balaban RS. Quantitative ^{1}H magnetization transfer imaging in vivo. Magn Reson Med 1991;17:304–314.
22. Yeung HN, Adler RS, Swanson SD. Transient decay of longitudinal magnetization in heterogeneous spin systems under selective saturation, 4: reformulation of the spin-bath-model equations by the Redfield-Provotorov theory. J Magn Reson A 1994;106:37–45.
23. Morrison C, Stanisz G, Henkelman RM. Modeling magnetization-transfer for biological-like systems using a seminisolid pool with a super-Lorentzian lineshape and dipolar reservoir. J Magn Reson B 1995;108:103–113.
24. Hennig J, Nauerth A, Friedburg H. RARE imaging: a fast imaging method for clinical MR. Magn Reson Med 1986;3:823–833.
25. Wolff SD, Balaban RS. Magnetization transfer contrast (MTC) and tissue water proton relaxation in vivo. Magn Reson Med 1989;10: 135–144.
26. Pike GB, Hu BS, Glover GH, Enzmann DR. Magnetization transfer time-of-flight magnetic resonance angiography. Magn Reson Med 1992;25:372–379.
27. Santyr GE, Kelcz F, Schneider E. Pulsed magnetization transfer contrast for MR imaging with application to breast. J Magn Reson Imaging 1996;6:203–212.
28. Meyerhoff DJ. Proton magnetization transfer of metabolites in human brain. Magn Reson Med 1999;42:417–420.
29. Petrella JR, Grossman RI, McGowan JC, Campbell G, Cohen JA. Multiple sclerosis lesions: relationship between MR enhancement pattern and magnetization transfer effect. AJNR Am J Neuroradiol 1996;17: 1041–1049.